Red Phosphorus-Induced Transformation of Gold Mesh into Crystalline Gold Phosphide Mesh

Hajime Suzuki Shusaku Shoji Fernando Garcia-Escobar Tomoya Tashiro Hideki Abe* Keisuke Takahashi**

H. Suzuki*, F. G. Escobar, T. Tashiro, K. Takahashi*
Address
Department of Chemistry, Hokkaido University, North 10, West 8, Sapporo 060-0810, Japan
Email Address
suzukihazime@eis.hokudai.ac.jp
keisuke.takahashi@sci.hokudai.ac.jp
S. Shoji, H. Abe*
Address
National Institute for Materials Science, 1-2-1 Sengen, Tsukuba, Ibaraki 305-0047, Japan
Email Address
abe.hideki@nims.go.jp
K. Takahashi*
Address
Institute for Chemical Reaction Design and Discovery, Hokkaido University, Kita 21, Nishi 10, Kita-ku, Sapporo, Hokkaido, 001-0021, Japan Email Address
keisuke.takahashi@sci.hokudai.ac.jp

Keywords: *Gold Phosphide,Materials Synthesis, Density Functional Theory, Macroscopic Crystalline*

Among transition metal phosphides, Gold phosphide (Au_2P_3) is particularly uncommon and lacks established synthesis methods for large-scale or structurally controlled materials, thus hindering its functional applications. This study introduces a synthetic strategy involving annealing gold mesh in red phosphorus vapor within a sealed quartz tube reactor, enabling a direct structural transformation into crystalline Au_2P_3 while preserving macroscopic geometry. Comprehensive characterization using XRD, SEM, EDS, and XPS confirms successful formation, revealing covalent Au–P bonding and a semiconducting nature validated by density functional theory (DFT) simulations, which accurately predict lattice parameters and electronic properties. This method opens possibilities for practical applications of Au_2P_3.

1 Introduction

Gold phosphides remain an underexplored class of compounds compared to their transition metal counterparts, despite gold's distinct electronic structure and chemical inertness[1, 2, 3]. Among them, Au_2P_3 is particularly rare, with limited reports focused primarily on crystallography and no established synthesis strategies for controlled morphology or large-scale structures. No functional applications have yet been demonstrated for Au_2P_3, largely due to challenges in synthesizing phase-pure material and inaccessibility of defined geometries. Recent advances in phosphidation chemistry, especially involving red phosphorus, have enabled the conversion of various metals into their corresponding phosphides[4, 5, 6]. However, such methods typically produce nanoparticles, thin films, or powders, and have not been extended to macroscale metallic substrates. Direct structural transformation of metallic gold into a crystalline gold phosphide structure with preserved macroscopic architecture has not been previously reported. Here, gold phosphorus is used to transform macroscopic gold mesh to Au_2P_3 method via gas flow reactor.

2 Materials Synthesis

Au_2P_3 mesh is synthesized by annealing Au mesh in phosphorus vapor. A quartz tube with an outer diameter of 15 mm, a wall thickness of 1 mm, and a length of 100 mm is selected as the growth container, which is dried in oven after cleaning. Red phosphorus (50 mg, RP, 99.9999%, FURUUCHI CHEMICAL), quartz cotton, and Au mesh (300 mg, 99.95%, THE NILACO CORPORATION) are put into a quartz

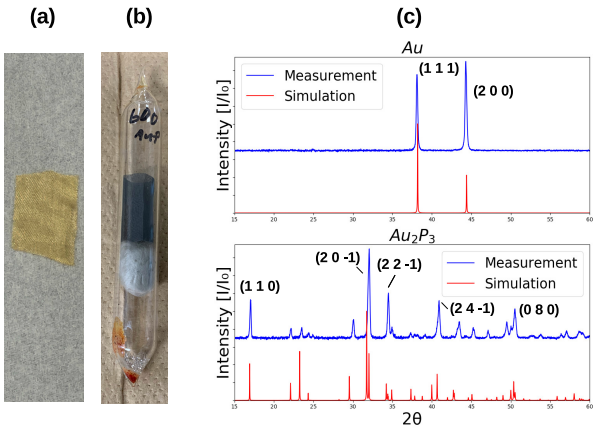

Figure 1: (a)Au mesh before reaction. (b)Gold phosphide (Au_2P_3) mesh in quartz tube. (c)XRD patterns of Au and Au_2P_3 mesh. Blue lines represent measured peaks and red lines represent simulated peaks.

tube. After being sealed under a vacuum (<10 Pa) using rotary pump and turbo molecular pump, the quartz tube is put into the tube furnace. RP is located in the low-temperature zone of quartz tube, and Au mesh is in the high-temperature zone. The reactor is heated to 600 °C at a rate of 10 °C/min from room temperature to avoid cracking of the material and kept for 1 h of heat preservation at this temperature. The quartz tube after reaction is shown in Fig. 1(b). The black mesh is Au_2P_3 and red chunk is white phosphorus. Au_2P_3 mesh is taken from quartz tube and washed by water to remove white phosphorus. The Au_2P_3 samples are extracted from the sealed quartz tubes under extra careful precautions.

3 Result and Discussion

X-ray diffractometers (XRD, Rigaku, MiniFlex600), scanning electron microscope (SEM, Hitachi High-Tech, SU1510), and X-ray energy scattering spectroscope (EDS) are performed in order to analyze the size, morphology, and composition of sample. The XRD pattern shows sample has Au_2P_3 peaks as shown in Fig. 1(c), which correspond to previous work[7]. SEM images are acquired using an accelerating voltage of 20 kV under a vacuum of 30 Pa. The sample for SEM is coated by platinum to improve electronic conductivity. SEM image and EDS spectrum indicate that Au_2P_3 crystal size is ∼10 μm and the ratio of P/Au is 1.26 as shown in Fig. 2(a).

X-ray photoelectron spectroscopy (XPS, JEOL, JPS-9200) with a Mg-Kα X-ray source (10 mA, 10 kV) is performed in order to analyze the surface electron states of Au_2P_3 as shown in Fig. 2(e)(f). The result indicates that the surface electron state of Au_2P_3 is characterized by Au 4f peaks at 83.4 eV and 87.1 eV and P 2p peaks at 128.7 eV and 133.5 eV. The Au peaks are shifted to lower binding energies relative to metallic Au (∼ 84 eV for $4f_{7/2}$ and ∼ 88 eV for $4f_{5/2}$), suggesting covalent environment around the Au atoms[8]. Meanwhile, the primary P peak at 128.7 eV is comparable to the peak observed in typical metal phosphides (∼ 129 eV), and the higher-energy peak at 133.5 eV is attributed to surface-oxidation-induced phosphate species[8]. These observations imply that Au_2P_3 forms covalent bonds rather than ionic bonds.

The density functional theory (DFT) calculation are confirmed through direct comparison with experimental measurements. The grid-based projector augmented wave software package (GPAW) within is implemented[11]. The exchange–correlation of Perdew–Burke–Ernzerhof is implemented with spin polarization[1 Grid spacing is set to 0.20 $\mathring{A}$ and 4x4x4 special k points of the Brillouin zone sampling is applied [13]. The relaxation procedure is executed until the forces on each atom are smaller than 0.10 eV$\mathring{A}^{-1}$. Bader charge analysis is implemented to understand the charge transfer [14, 15]. Both DFT calculations and X-ray diffraction (XRD) analysis reveals matching lattice constants; the DFT-computed values are a = 5.89 Å, b = 14.43 Å, c = 4.73$\mathring{A}$, while experimental values are a = 5.86 Å, b = 14.43 Å, c = 4.67$\mathring{A}$, indicating reliable reproduction of the crystal structure, as shown in Fig. 3(a). Moreover, X-ray diffraction

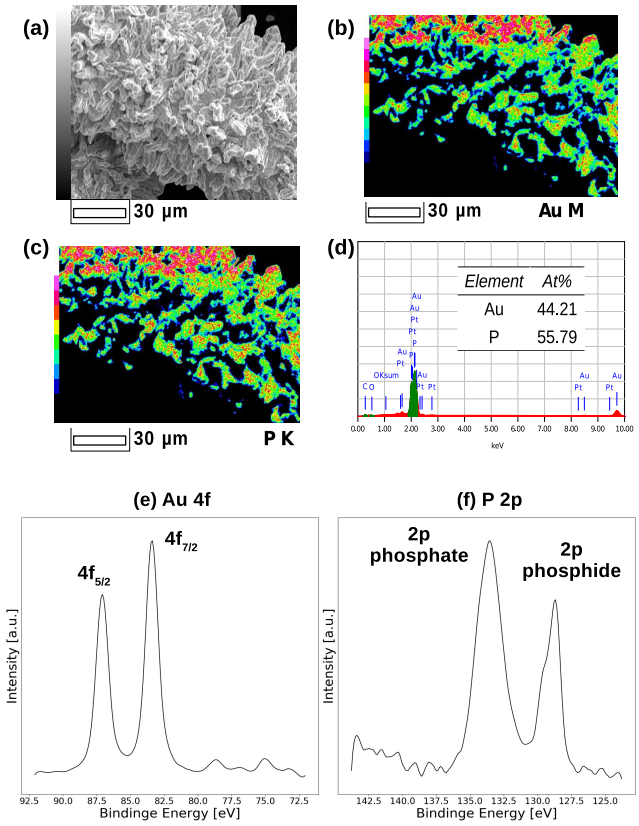

Figure 2: The SEM image and EDS spectrum of Au_2P_3. (a)SEM image of the Au_2P_3 mesh. (b)Element scanning mapping of Au element and (c)P element of Au_2P_3. (d)Element contents of Au and P in the sample. (e)(f)XPS patterns of Au 4f and P 2p orbitals of Au_2P_3.

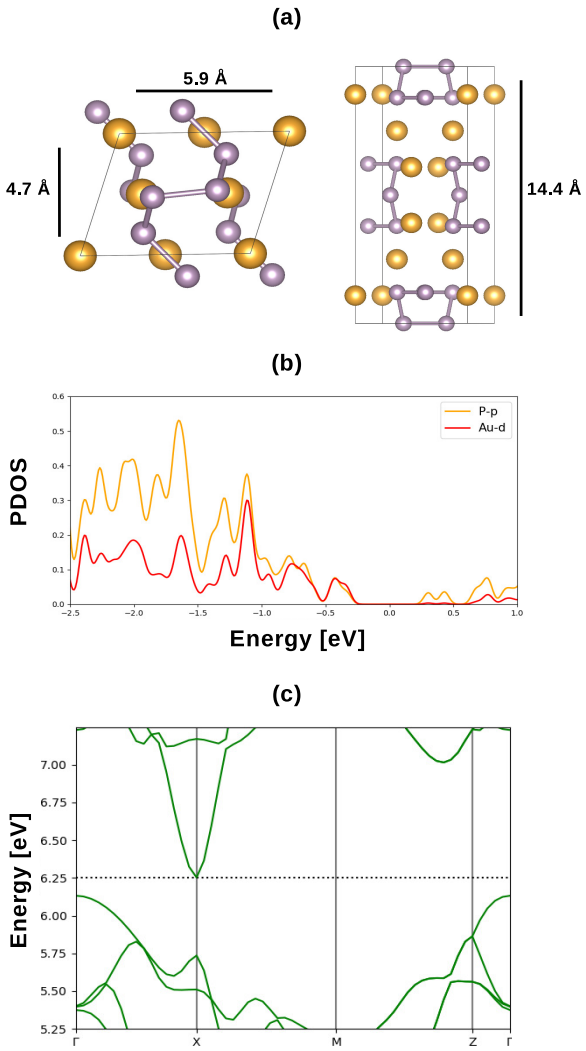

Figure 3: (a)The illustration of Au_2P_3 structure. Atomic color code: yellow-gold, purple-phosphorus. (b)Projected density of states (PDOS) between Au-d and P-p states. (c)The electronic band structure of Au_2P_3. Dot line indicates Fermi level.

patterns are simulated using visualization for electronic and structural analysis (VESTA)[16], as shown in Fig. 1(c). The result shows agreement with experimental data, reinforcing structural accuracy predicted by the computational approach.
Electronic structure analysis using Bader charge distribution and projected density of states (PDOS) further aligns with X-ray photoelectron spectroscopy (XPS) findings. The Bader analysis yields subtle charge transfers of approximately +0.1e on phosphorus (P) atoms and -0.1e on gold (Au) atoms, indicative of a covalent bonding character. PDOS shows overlapping between Au-d and P-p states in the range of -1.1 to -0.4 eV, as shown in Fig. 3(b). The result supports the covalent bonding character, indicating agreement with the Bader analysis and XPS measurements.
The electronic band structure is demonstrated to understand a electronic nature of Au_2P_3, as shown in Fig. 3(c). The result indicates an indirect band gap between the Γ and X points. The band gap is calculated to be 0.12 eV using PBE functional, while employing the GLLB-SC functional yields a band gap of 0.17 eV. Materials with an indirect band gap of 0.17 eV are ideally suited for mid-infrared photodetectors[9, 10]. Futher modification such as doping could increase the conductivity of Au_2P_3. Thus, Au_2P_3 exhibits promising semiconducting behavior with an indirect band gap.

4 Conclusion

In conclusion, this work demonstrates the direct transformation of macroscopic gold mesh into crystalline Au_2P_3 by annealing in phosphorus vapor. It is noteworthy that the synthesized Au_2P_3 mesh retains its crystalline structure even after several months of storage in air. The synthesized Au_2P_3 mesh exhibits crystallinity and covalent bonding characteristics, validated experimentally via XRD, SEM, EDS, and XPS. DFT simulations complement these findings by precisely reproducing lattice parameters and predicting an indirect semiconducting band gap, confirming the covalent bonding nature. This synthesis approach significantly advances the material availability and practical use of Au_2P_3, overcoming historical challenges related to producing structurally defined and phase-pure gold phosphide materials. The combination of experimental and theoretical analyses provides robust evidence supporting potential electronic applications for Au_2P_3.

Acknowledgements
This work is funded by the Japan Science and Technology Agency(JST) ERATO grant number (JPMJER1903), and JST Mirai Program Grant Number (JP-MJMI25G1), JSPS KAKENHI Grant in Aid for Scientific Research (B) Grant Number (JP23H01762) and (24K01241), Grant-in-Aid for JSPS Fellows Grant Number (JP24KJ0272).

References

References

[1] N. Panyala, J. Havel, *Rapid Commun. Mass Spectrom.* **2012**, *26*, 1100–1108.

[2] S. Carenco, I. Florea, O. Ersen, *New J. Chem.* **2013**, *37*, 1231–1237.

[3] D. Fernando, T. Nigro, I. Dyer, S. Alia, B. Pivovar, Y. Vasquez, *J. Solid State Chem.* **2016**, *242*, 182–192.

[4] K. Bhunia, M. Chandra, S. Sharma, D. Pradhan, S. Kim, *Coord. Chem. Rev.* **2023**, *478*, 214956.

[5] L. He, J. Guo, S. Liu, F. Wang, X. Li, Z. Su, *J. Alloys Compd.* **2024**, , 174924.

[6] Z. Xing, Q. Liu, A. Asiri, X. Sun, *ACS Catal.* **2015**, *5*, 145–149.

[7] W. Jeitschko, M. Moller, *Acta crystallographica. Section B.* **1979**, *35*, 573–579.

[8] J. Rumble Jr, D. Bickham, C. Powell, *Surf. Interface Anal.* **1992**, *19*, 241–246.

[9] S. Hou, L. Han, S. Zhang, L. Zhang, K. Zhang, K. Xiao, Y. Yang, Y. Zhang, Y. Wen, W. Mo, *Adv. Sci.* **2025**, *12*, 2415518.

[10] M. Chou, R. Bansal, Y. Jheng, G. Sun, W. Du, S. Yu, G. Chang, *Adv. Photonics Res.* **2025**, *6*, 2400155.

[11] J. Mortensen, L. Hansen, K. Jacobsen, *Phys. Rev. B* **2005**, *71*, 035109.

[12] J. Perdew, K. Burke, M. Ernzerhof, *Phys. Rev. Lett.* **1996**, *77*, 3865.

[13] H. Monkhorst, J. Pack, *Phys. Rev. B.* **1976**, *13*, 5188.

[14] G. Henkelman, A. Arnaldsson, *Comput. Mater. Sci.* **2006**, *36*, 354–360.

[15] W. Tang, E. Sanville, G. Henkelman, *J. Phys.: Condens. Matter.* **2009**, *21*, 084204.

[16] K. Momma, F. Izumi, *J. Appl. Crystallogr.* **2011**, *44*, 1272–1276.

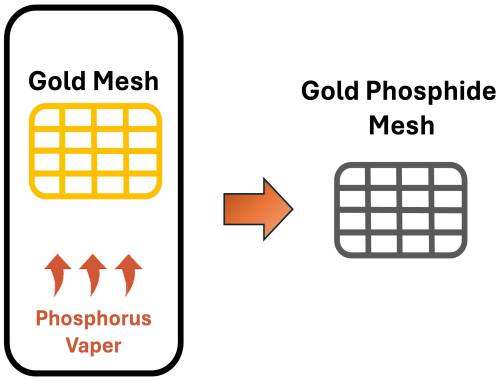

Figure 4: Table of contents